

Project Number: RG1-B016

QUARTZ CRYSTAL MICROBALANCE MEASUREMENTS OF
ADSORPTION POTENTIAL WELL DEPTHS

A Major Qualifying Project Report:

submitted to the Faculty

of the

WORCESTER POLYTECHNIC INSTITUTE

in partial fulfillment of the requirements for the

Degree of Bachelor of Science

by

Ryan Foltz

Date: April 1 2004

Approved:

Professor Rafael Garcia, Advisor

Abstract

Changes in the resonant frequency of a quartz crystal microbalance (QCM), can be used to measure film thicknesses on the order of 0.1 monolayer or less that are adsorbed on the microbalance's electrode surfaces. The well-depth of the adsorption potential for molecules on a flat surface is a key parameter for determining the wetting transition temperature for molecules on that surface. However, it is a difficult quantity to predict with precision using theoretical models. A QCM was used to determine the well-depth of the adsorption potential for nitrous oxide and other polar molecules on flat surfaces. We compare our data with available theoretical predictions.

Acknowledgments

The author would like to thank Professor Rafael Garcia who made this project possible and provided guidance throughout. Additional thanks to Jacqueline Malone and the WPI machine shop.

TABLE OF CONTENTS

	Page
Abstract	ii
Acknowledgments	iii
1. INTRODUCTION	1
2. THE APPARATUS	6
2.1. The Cell	6
2.2. The Pressure Manifold	8
2.3. The Electronics	11
2.4. The Computer Program	14
3. EXPERIMENT AND ANALYSIS	19
3.1. Determining Film Thickness	20
3.2. Corrections for Other Factors	21
3.3. Determining the Potential Function	23
4. CONCLUSIONS	29
Appendix A	31
Appendix B	33
References	34

1. INTRODUCTION

A liquid in contact with a substrate may either bead up to form a droplet or spread out to form a thin film. A droplet is described as nonwetting and can be characterized by the liquid-surface contact angle pictured in Fig. 1.1. A liquid that spreads to form a thin film is described as wetting.

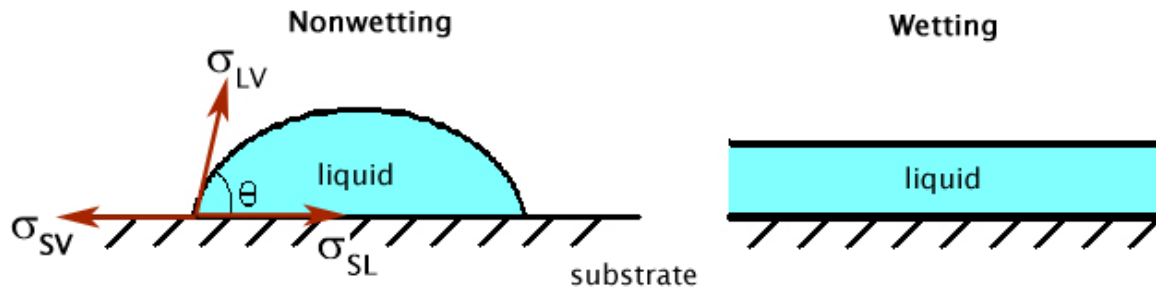


Figure 1.1: A wetting and nonwetting liquid are pictured on a substrate. The nonwetting liquid forms a contact angle θ with the surface. Also pictured are the various surface tensions $\sigma_{LV}, \sigma_{SL}, \sigma_{SV}$. [10]

The a liquid's contact angle on a surface can be described in terms of the various surface tensions by means of Young's equation [1]:

$$\sigma_{SV} - \sigma_{SL} = \sigma_{LV} \cos \theta \quad (1.1)$$

Difficulties involved in determining all three surface tensions theoretically prevent the use of this equation for our purposes. However, Young's equation can be re-cast in terms of a molecule-surface attractive potential V [1]:

$$\sigma_{SL} - \sigma_{SV} = \sigma_{LV} \frac{\Delta\rho}{M} \int_{z_{\min}}^{\infty} Vdz \quad (1.2)$$

where $\Delta\rho$ is the difference in densities between the liquid and vapor phases of the liquid, z_{\min} is the minimum of the potential function and M is the molecular weight of the liquid.

Substituting Eq. 1.2 into Eq. 1.1 yields an expression for the contact angle in terms of the molecule-surface attractive potential:

$$\cos \theta = -1 - \frac{\Delta\rho}{\sigma_{LV} M} \int_{z_{\min}}^{\infty} Vdz \quad (1.3)$$

From this it follows that we can predict the wetting behavior of a liquid on a substrate if the potential function is known.

It has been shown [2] that a nonwetting liquid on a substrate will eventually wet the surface above a wetting temperature T_w . This wetting transition occurs as θ approaches zero, and can be theoretically predicted from Eq. 1.3 for a known molecule-surface attractive potential. A generic phase diagram showing this wetting transition is given in Fig. 1.2.

This wetting transition has been observed [3] for various liquids and substrates, but has not been observed for polar liquids or wetting transitions near room temperature. It is expected that wetting transitions for polar liquids will exhibit new phenomena [4], as the potential function for a polar liquid can be highly temperature dependent leading to more complex interactions with the

substrate and other molecules.

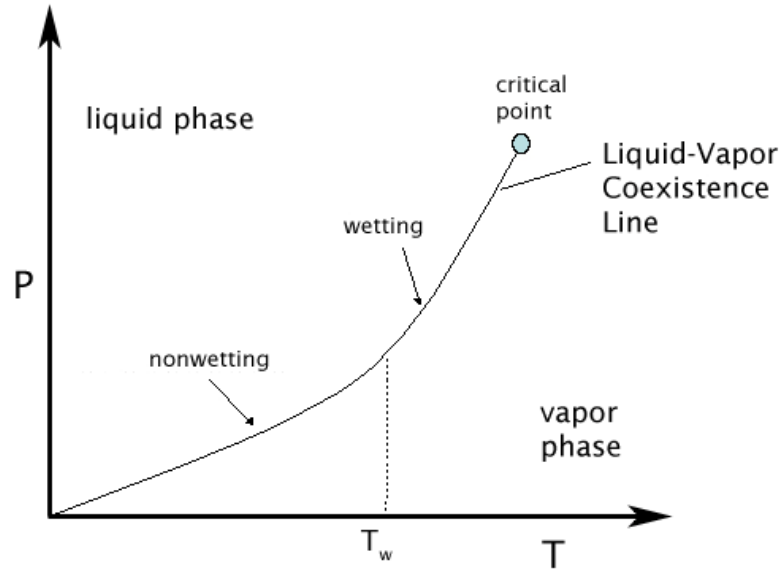


Figure 1.2: A phase diagram demonstrating the wetting temperature T_w .

Nitrous oxide is an attractive substance for studying wetting transitions in a polar liquid. Nitrous oxide is polar and has a critical temperature of 36.4 degrees Celsius, close to room temperature. Nitrous oxide's critical pressure is 71.6 atmospheres [5]. Because of these properties, we expect that a novel observation of a room-temperature wetting transition in a polar liquid can be made for nitrous oxide.

Gatica *et. al.* [6] predict the wetting temperature for water on gold to be between 350 and 500 degrees Kelvin. The wetting temperature T_w for nitrous oxide on various substrates is predicted only with great uncertainty due to varying estimates of the molecule-surface attractive potential.

Previous experiments with wetting transitions in nitrous oxide

have failed to observe wetting on sapphire for temperatures up to 35.4 degrees Celsius [11]. This temperature is close to the critical point of nitrous oxide. A more confident prediction for the wetting temperature of nitrous oxide would assist in interpreting the data from these experiments. Some images from these experiments are shown in Fig. 1.3.

The goal of this MQP was to experimentally establish parameters for the molecule-surface attractive potential for nitrous oxide on gold and thus predict the wetting temperature with greater precision. This can be accomplished by measuring thin-film adsorption onto a quartz crystal microbalance (hereafter QCM) at low pressures. At low pressures, we can apply Henry's law to relate the thickness of a thin film to the potential function:

$$d = \int \rho V(z) dz = \int_{z \text{ min}}^{\infty} \rho_0 e^{\frac{-V(z)}{k_B T}} - 1 dz \quad (1.4)$$

where d is the film thickness in mass per.

By driving the QCM with an AC signal, we can observe a mass-loading effect on the QCM by measuring changes in its resonant frequency [7], and therefore determine the film thickness d. With this data we would then be able to establish more precise values for the parameters of the potential function.

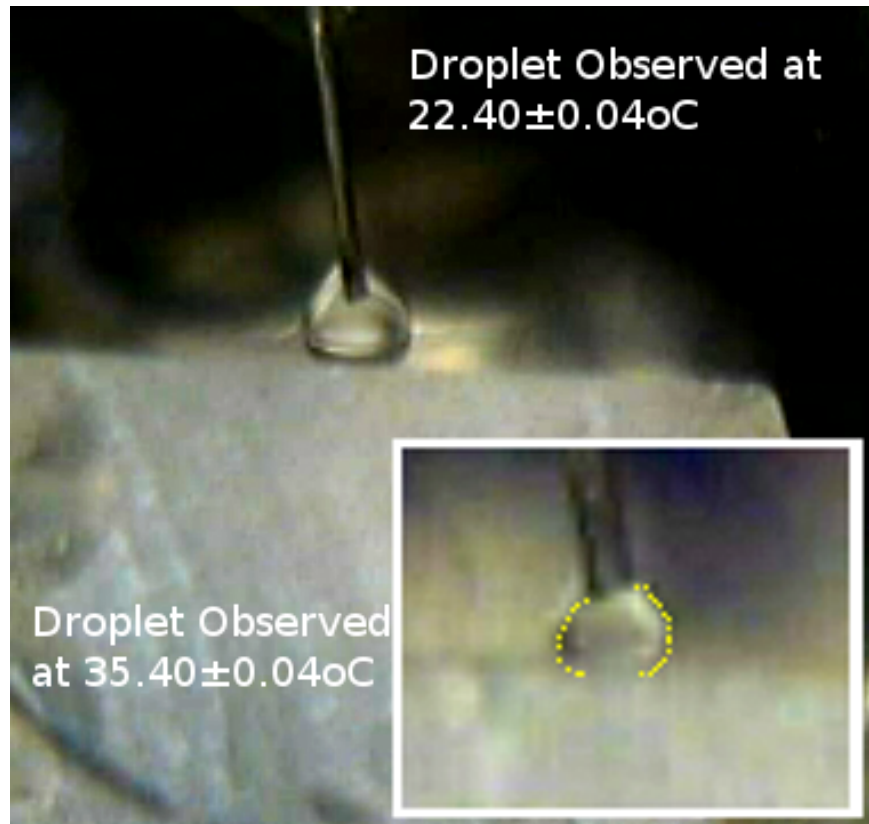


Figure 1.3: Nonwetting droplets of nitrous oxide on a sapphire substrate observed at various temperatures [11].

2. THE APPARATUS

A new experimental apparatus needed to be constructed for the purposes of this experiment. The data we intended to gather required precise control of the temperature and pressure of the QCM's environment. Additionally, we would need to control the amount of nitrous oxide introduced, and have electronics set up to interface with the QCM.

2.1 The Cell

The cell was machined prior to the beginning of this MQP, although it was not assembled. As it was originally designed for water wetting experiments, the cell was intended for temperatures up to 500 degrees kelvin and pressures as high as 200 atmospheres. The cell was suited for our particular experiment, which was to take place at low pressures and near room temperature.

The cell was built around a section of 1" diameter stainless steel tubing (see Fig. 2.1.) A capillary was drilled in the body of the cell to allow control of the cell pressure and to introduce nitrous oxide; connection to the capillary is provided by a 1/16" stainless steel swagelok tube fitting. Electronic connections are mediated by Ceramaseal electrical feedthroughs held in place with swagelok fittings. The front end of the cell was sealed by a sapphire window to allow viewing of the QCM while the rear of the cell was

sealed by a 1" diameter stainless steel swagelok tube cap.



Figure 2.1: The cell is pictured with the capillary on top, electrical feedthroughs to the sides, and the window in front. The rear cap is not pictured. Picture taken from Waegall's MQP thesis [10].

Although the necessary parts were assembled prior to this MQP by Mordecai Waegell [10], we needed to assemble the cell with the QCM inside and connected to the electrical feedthroughs. As the introduction of air would corrupt the experiment, thorough leak testing was also required. Previous experiments in this area, as well as our use of epoxy and solder led us to suspect that contamination of the nitrous oxide might also confound the data; as such, the assembly of the cell took place in a clean room to minimize exposure to dust, oils and other contaminants.

The swagelok connections were made air-tight by screwing the stainless steel ferrules onto the surface to be sealed. The QCM needed to be inserted in such a manner that its two connectors could be soldered to the copper feedthroughs while not shorting to the cell or each other. The final process involved soldering the connectors and feedthroughs outside the cell, and folding the wires back into the cell to allow for the rear cap to seal the cell.

Ensuring that the cell was airtight proved to be the biggest obstacle of the assembly phase. Upon discovering leaks, the cell needed to be disassembled and re-assembled twice in an effort to eliminate leakage. This will be discussed in more detail in section 2.2.

Although this cell design was employed in tests leading up to the final experiment, a different cell design was used for gathering data at zero degrees Celsius. The new cell design did not feature a window or the swagelok feedthroughs, but the function remained the same. All of the data used in the analysis was obtained using this new cell design.

2.2 The Pressure Manifold

The pressure manifold was designed to connect the cell to the nitrous oxide. To perform the experiment, we needed to be able to control the dosing of nitrous oxide as well as measure the pressure in the cell. Furthermore, the cell would need to be occasionally

connected to a diffusion pump in order to remove air and other potential contaminants as well as residual nitrous oxide from successive experiments.

All connections were made with 1/16" stainless steel tubing through High Pressure connectors, joints and valves. Forming a connection required the cutting and deburring of a section of tubing, and then screwing the tubing in place with a High Pressure connector and ferrule. Although initial difficulties in the construction process necessitated the re-forming of all connections, the High Pressure connectors and valves proved to be very robust, maintaining a seal through multiple disassembles and a range of pressures.

The MKS Baratron capacitance monometer pressure gauges, one rated at ten Torr and the other rated at one thousand Torr, were chosen to cover a potential range from zero Torr to one thousand Torr. This corresponds to a range from vacuum to a little over one atmosphere. The gauges themselves were temperature-controlled for greater precision and employed stainless steel connectors and a plastic alloy diaphragm to prevent contamination. In practice the gauges allowed measurements from 0.01 Torr to 1000 Torr.

The initial design called for a simple four-way connection between the cell, the ten-Torr pressure gauge, a valve leading to the diffusion pump, and a valve leading to the nitrous oxide. The nitrous oxide was controlled through a pressure regulator connected to a series of two valves; this allowed for small amounts of nitrous oxide to be introduced slowly, by staggering the valves. By

In the later stages of the experiment, the pressure manifold was redesigned to connect the ten-Torr gauge to the nitrous oxide buffer and the thousand-Torr gauge to the cell. This served the dual purpose of allowing us to record a broader range of pressures in the cell as well as control the introduction of nitrous oxide with greater precision. This final design is pictured in Fig. 2.2.

Both designs incorporated a long section of thin tubing connecting the bulk of the cell's volume to the diffusion pump. Because of this bottleneck effect, pump-down times were exacerbated, requiring pumping intervals of up to twenty-four hours between experiments.

After all the components were connected as needed, leak testing proceeded by use of a Veeco diffusion pump leak detector. The leak tester works in principle by detecting traces of helium brought through the diffusion pump: by constantly pumping on the cell and spraying helium on a leak, the helium would be sucked into the pump and then indicated visually on a display. The entire process of leak testing the pressure manifold required two weeks, from the initial construction of the manifold to the realization of an airtight setup. It was during this phase that leaks in the cell were detected; resolving the leaks required the tightening of the swagelok fittings as well as the replacement of a defective electrical feedthrough.

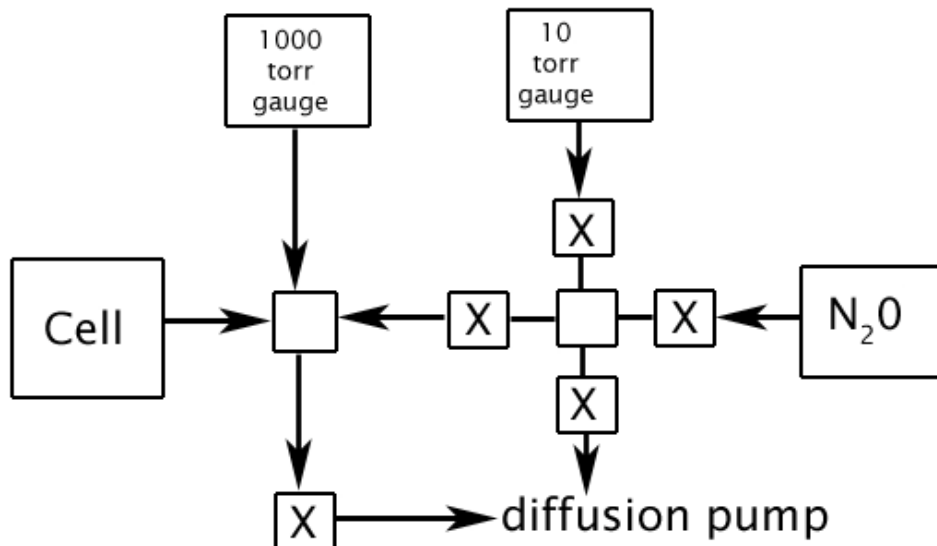


Figure 2.2: Diagram showing the pressure manifold. Valves are indicated by an X, arrows indicate direction of flow. The cell can be isolated from the nitrous oxide and the pump, and nitrous oxide can be introduced in small quantities through the buffer.

2.3 The Electronics

The electronics were necessary to provide a driving frequency input for the QCM, and to interpret its output signal. For this, we used a high-frequency function generator and a high-frequency analog lock-in amplifier. These electronics are shown in Fig. 2.3.

The Hewlett-Packard 3325A function generator was capable of frequencies from 1 microhertz to 50 megahertz. The lock-in amplifier, a Princeton Applied Research Model 5202, was fed the output signal from the QCM with the driving frequency from the function generator as a reference, separating the QCM output into two signals: one

response in phase with the driving frequency, and one response ninety degrees out of phase with the driving frequency. This data was used to control a feedback loop that would maintain the driving frequency at resonance; this is discussed further in section 2.4.

To connect the function generator and lock-in amplifier to the cell, we used stripped coaxial cable. The leads from the cables were soldered to the copper feedthroughs on the cell and insulated in heat-shrinking tubing. The coaxial grounds were then connected to each other and the cell to prevent ground loop noise.

In addition to the main electronics, we also employed a Lakeshore Model 340 temperature controller to interface with a platinum resistor thermometer that was epoxied to the cell. Initial plans called for the use of the Lakeshore's heater control capabilities; however, we found that for our cell and heater tape, the power output of the Lakeshore was insufficient to maintain a constant high temperature above forty degrees Celsius. Later we attempted control of the heater tape by connecting it to a direct current power supply, this also was impractical due to electrical noise. Ultimately, a stable temperature was achieved by immersing the cell in an ice-water bath that remained at a constant zero degrees Celsius.

All the data gathered from the sensors and QCM output was sent to a nearby computer through a GPIB connection. Some of the instruments, such as the function generator and temperature controller, accepted GPIB connections directly. For analog components

and components lacking GPIB interfaces, the outputs were connected to GPIB-capable voltmeters. The MKS PDR2000 pressure gauge readout and power supply required the soldering of a special connector that allowed an analog connection to a GPIB voltmeter. The computer's handling of this data will be examined in section 2.4.

The voltmeters used were Hewlett-Packard models 3468A and 34401A multimeters. Both models were capable of GPIB interface, and were configured to allow the greatest precision.

Ultimately the obstacle that was most difficult to overcome was electrical noise. As our function generator had a precision of eleven digits, and we were looking for changes in the resonant frequency on the order of tenths of a hertz, we needed to minimize the electrical noise below this threshold to maximize the use of our equipment. Although never fully eliminated, the noise was reduced significantly by connecting the grounds of the equipment, taping down the cables and providing a humidifier. Besides the expected electrical noise, we also observed random "walks" as signals would drift, and random "jumps" or discontinuities when a signal would suddenly assume a new value. Oftentimes the jumps would be observed switching between two distinct values; no explanation for this noise was discovered, but it was sufficiently minimized to allow us to conduct the experiment.



Figure 2.3: Pictured are the electronics used in gathering data. The lock-in amplifier (top right) and function generator (bottom right) are located next to the temperature controller (bottom left) and two agilent multimeteres (top left).

2.4 The Computer Program

As described in section 2.3, the computer interfaced with a variety of instruments through a GPIB port. The nature of GPIB interface allows for daisy-chaining a large number of instruments accessible by distinct ID numbers. Typically the computer would poll a given instrument which would then return the value displayed, although the GPIB interface could also be used to pass commands to

the instruments and change their settings.

To manage all of the GPIB commands and data, we needed to write a computer program. The program was written in LabView version 8.0, and consisted of two major parts: one would constantly run a feedback loop to maintain the driving frequency at resonance while the other would intermittently record the various data.

The feedback loop relied entirely on the quadrature output from the lock-in amplifier. As can be seen in Fig 2.4, the quadrature output is zero at resonance, and very nearly linear in the immediate region of the resonant frequency. For this reason we used the quadrature response to control the feedback loop; although it is possible in theory to seek a maximum for the in-phase response, the peak is very narrow and the response does not vary linearly in its region, making such a control scheme difficult. The feedback loop is represented in Fig. 2.5.

The phase offset of the lock-in amplifier was set so that the quadrature response would be positive above the resonant frequency. From this, the computer would read the magnitude of the quadrature response, multiply it by an adjustable factor, and then add it to the current driving frequency. This simple method ensured that the function generator frequency would constantly be adjusted to achieve the resonant frequency. With a high time constant setting on the lock-in amplifier and a low adjustment factor in the feedback loop, the quadrature response would be smoothly varying around zero and the resonant frequency would not be over- or under-shot.

The data recording loop would periodically poll the instruments to obtain readings on the pressure and temperature, as well as the in- and out-of-phase responses of the QCM, and record these values to a tab-delineated text file. The time interval at which the readings were taken was adjustable, usually data was recorded every two to five minutes. The recorded data could be easily transferred over a network or imported into various software for analysis.

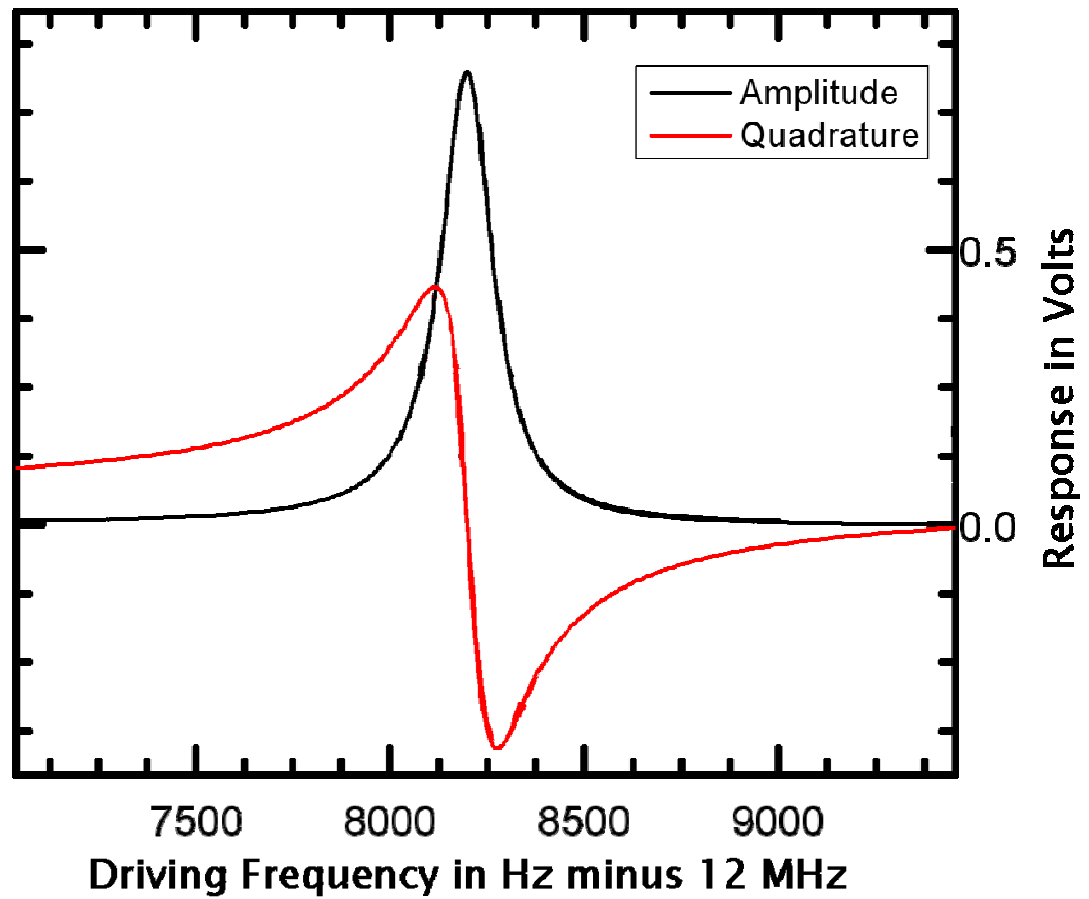


Figure 2.4: The in- and out- of phase response of the QCM over a range of driving frequencies near resonance. Note that the quadrature response is zero when at resonance.

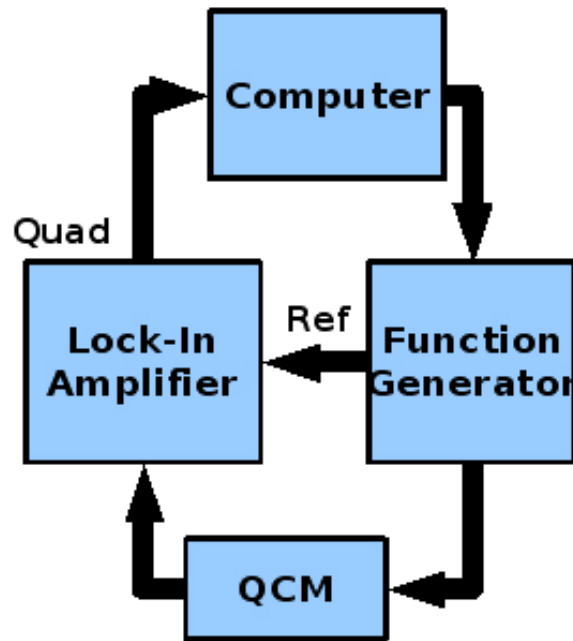


Figure 2.5: The function generator drives the QCM, the response of which is input into the lock-in amplifier with the driving frequency as reference. The quadrature response of the lock-in is used by the computer to adjust the driving frequency of the function generator.

3. EXPERIMENT AND ANALYSIS

Time constraints and the technical difficulties outlined in sections 2.2 and 2.3 forced us to accept only one full data set at a temperature of 0 degrees Celsius. Nevertheless, analysis of this data was still possible though it lacked the verification that repeated experiments at different temperatures would yield. The data from this experiment, relating the change in the resonant frequency of the QCM to the pressure of the nitrous oxide can be found in Fig 3.1. Specific blow-ups of the high- and low-pressure regimes can be found in Appendix A.

Change in Frequency vs. Pressure for T=273.15 K

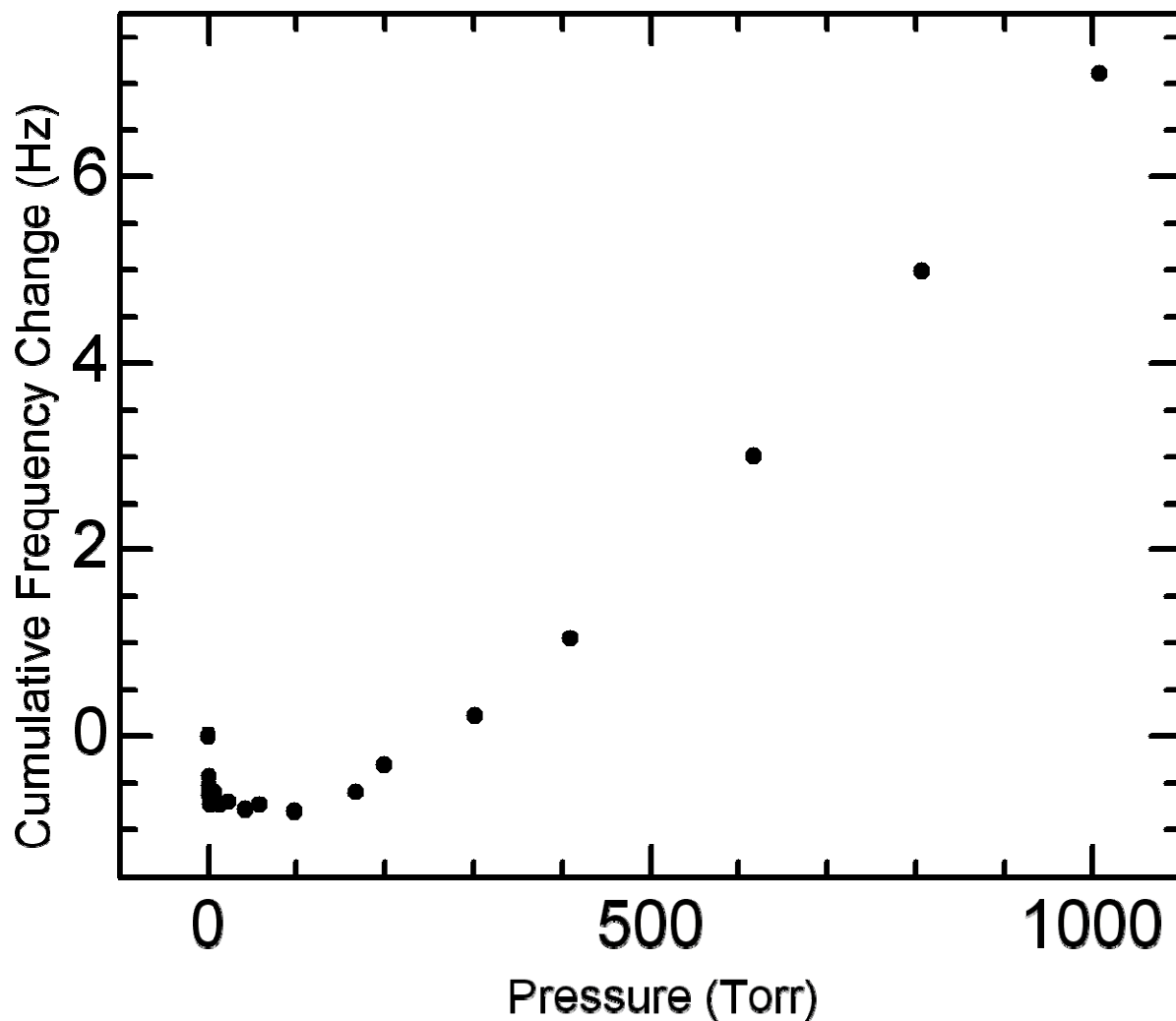


Figure 3.1: The cumulative change in resonant frequency is plotted versus the pressure in the cell.

3.1 Determining the film thickness

As was mentioned in section 1, the adsorbed film thickness can be determined by the equation

$$d = -K\rho_q t_q \frac{\Delta f}{f_0} \quad (3.1)$$

where ρ_q is the density of quartz, t_q is the thickness of the QCM, Δf is the cumulative change in frequency, f_0 is the initial resonant frequency, and K is a dimensionless quantity [7].

Note that the change in resonant frequency should be negative, i.e., the resonant frequency should decrease as nitrous oxide is adsorbed onto the gold electrodes of the QCM. A dimensional check reveals that the film thickness d is described in units of mass per area, which is consistent with Eq. 1.4. With this equation, we can combine with Eq. 1.4 to arrive at an expression relating the measured Δf to the desired potential function:

$$-K\rho_q t_q \frac{\Delta f}{f_0} = \int_{z_{\min}}^{\infty} \rho_0 e^{\frac{-V(z)}{k_B T}} - 1 dz \quad (3.2)$$

However, at this point it is worth noting that other environmental factors can influence the resonant frequency of the QCM. Before applying Eq. 3.2 to determine the potential function we must correct for these factors so that we know the change in resonant frequency due only to the mass-loading effect.

3.2 Corrections for Other Factors

The QCM exhibits a sensitivity in its resonant frequency to changes in pressure, temperature and environmental viscosity. This pressure dependence was examined by Stockbridge [8] and is simply a

linear effect that serves to increase the resonant frequency. We can describe this effect as

$$\Delta f_p = +0.018 \frac{\text{Hz}}{\text{Torr}} \quad (3.3)$$

The viscosity of the nitrous oxide vapor surrounding the QCM dampens the oscillations and lowers the resonant frequency. This effect is described by the equation

$$\Delta f_v = -\sqrt{\frac{f_0 \eta M}{4\pi R \rho_q^2 t_q^2 K^2}} \sqrt{\frac{P}{T}} \quad (3.4)$$

where η is the viscosity of nitrous oxide, R is the gas constant, P is the pressure in the cell and T is the temperature in degrees Kelvin [8].

Although the viscosity of nitrous oxide is also dependent on temperature and pressure, it changes very little in the regime we are considering and so we can treat it as a constant.

The QCM we used is an AT-cut quartz which is cut specifically to have very low temperature dependence. As we held the temperature constant throughout the experiment, the effect on the resonant frequency due to any fluctuations was negligible.

After determining these other effects, we can solve for the change in resonant frequency due to mass loading alone:

$$\Delta f_M = \Delta f - \Delta f_p + \Delta f_v \quad (3.5)$$

This equation along with Eq. 3.2 allows us to relate the potential function to our data.

3.3 Determining the Potential Function

Various parameterizations of the molecule-surface attractive potential have been suggested, but in general we can assume that the function takes the form

$$V = \frac{4C^3}{27D^2z^9} - \frac{C}{z^3} \quad (3.6)$$

This function is shown graphically in Figure 3.1.

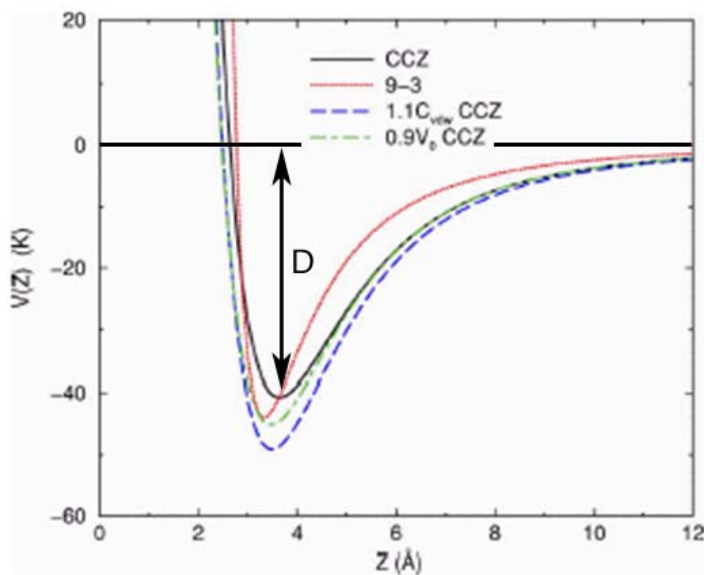


Figure 3.1: A plot of the potential function V . Various estimations of V are shown in different colors. The well-depth D is indicated graphically [6].

It can be seen that the potential function depends on two parameters, the Van Der Waals attraction coefficient C and the well-depth parameter D . The original purpose of the experiment was to determine D experimentally, with C known from theory. However, a theoretical determination of C proved to be difficult. Instead we employed an experimental determination of C .

At high pressures, the Van Der Waals attraction dominates the potential function, and we can use the relation [9]

$$d = \sqrt[3]{\frac{k_B T \ln\left(\frac{P_0}{P}\right)}{C}} \quad (3.7)$$

Our experiment recorded data at pressures up to 1000 Torr. For d values in this high-pressure regime, we can determine the Van Der Waals coefficient C graphically by plotting d versus $\sqrt[3]{\ln\left(\frac{P_0}{P}\right)}$. This is shown in Fig. 3.2.

The equation used to determine C in our experiment (Eq. 3.7) already assumes wetting behavior. Additionally, it is possible that the data we used to determine C was not at sufficiently high pressures, as this would also affect the result.

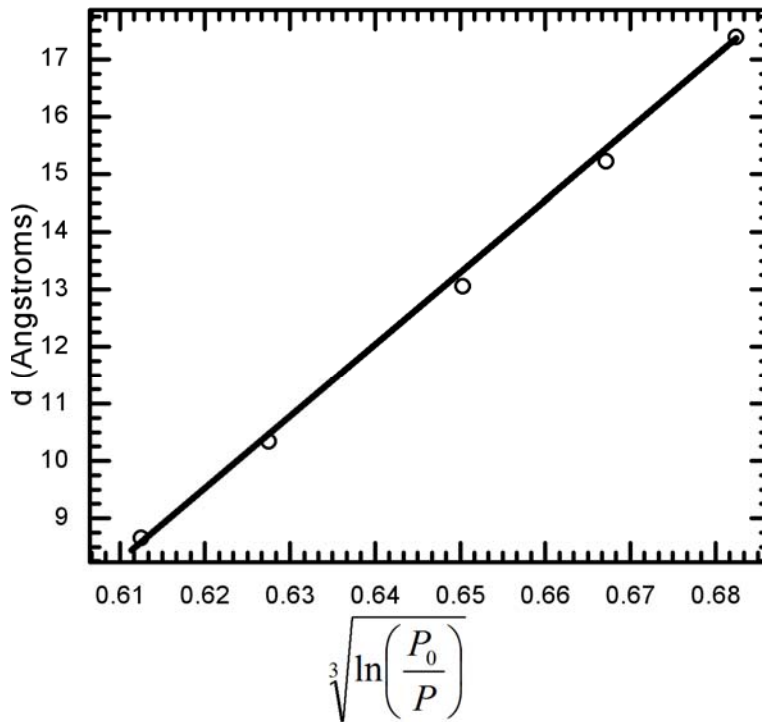


Figure 3.2: A linear fit of the data for the high-pressure regime. From the slope we can determine the parameter C.

Employing this method yielded a value for C of 49,300 eV cubic angstroms per atom (7.89×10^{-45} Joule meters cubed per atom.)

Equation 3.2 is difficult to deal with if we use the full form of the potential function (Eq. 3.6). We had originally tried approximating the potential function as a parabola (Eq. 1.4.) Although convenient to work with, this approximation breaks down for small D values, and does not apply for the value of C as we have determined it. Instead of approximating the function, we decided to solve the integral numerically by computer.

To do this, a MATLAB function was written to evaluate the specific integral for given values of C and D. By repeatedly

integrating over different values of D, we can determine for what values of C and D the equation holds:

$$I(C, D) = \int_{z \min}^{\infty} \rho_0 e^{\frac{-V(z)}{k_B T}} - 1 dz = \frac{df}{dP} \frac{K \rho_q t_q k_B T}{f_0 M} \quad (3.8)$$

By solving the right side of the equation, we can arrive at a dimensionless numerical value that the integral must equal. With the C value given above, successive iterations of the integral yields a D value of 1.22×10^{-5} eV per atom (1.95×10^{-24} Joules per atom.) The MATLAB code used to numerically solve the integral can be found in Appendix B.

Having determined values for C and D, we can now use the original equation (Eq. 1.3) to solve for the temperature at which the contact angle vanishes. Temperature dependence in this equation is introduced in the changing values of the surface tension and relative densities. We can solve for T_w by substituting Eq. 3.6 into Eq. 1.3 [6]:

$$M \frac{\sigma(T)}{\Delta \rho(T)} = \frac{1}{3.33} \sqrt[3]{CD^2} \quad (3.9)$$

For nitrous oxide, the values of σ and $\Delta \rho$ for different temperatures are well known [5]. We can solve this equation graphically (shown in Fig. 3.3,) and arrive at the corresponding T_w .

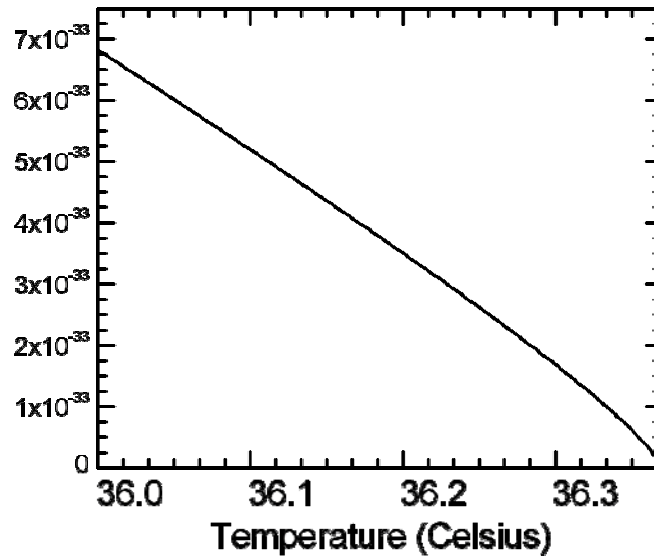


Figure 3.3: A plot of the function given by Eq. 3.9. The left scale represents the value for the left hand of the equation for nitrous oxide at different temperatures.

As nitrous oxide only has a liquid and vapor phase for temperatures above its freezing point and below its critical point, it is possible that there may be no solution to Eq. 3.9. For the given values of C and D, there is no solution; this implies that nitrous oxide wets gold at zero degrees Celsius.

The values found for D for different methods of calculation and values of C are shown in Table 3.1.

Table 3.1: Results for D for various values of C and solutions to Eq. 1.4

	Parabolic Approximation	Numeric Integration
Experimental C $C = 7.89 \times 10^{-45} \text{ Jm}^3/\text{atom}$	$D = 2.06 \times 10^{-26} \text{ J/atom}$ $T_w = 36.14 \text{ deg. C.}$	$D = 1.95 \times 10^{-24} \text{ J/atom}$ Wets
C for Water on Gold $C_{\text{H}_2\text{O}} = 2.63 \times 10^{-49} \text{ Jm}^3/\text{atom}$	$D = 5.97 \times 10^{-20} \text{ J/atom}$ Wets	$D = 4.76 \times 10^{-24} \text{ J/atom}$ Wets

4. CONCLUSIONS AND RECOMMENDATIONS

Several aspects of the stated results imply that the conclusions or analysis are suspect. The first thing to notice is that the experimentally determined value for the Van Der Waals coefficient C is several orders of magnitude higher than expected. For contrast, the C value for water on gold is only 1.64 eV angstroms cubed. As water is a polar molecule, the C value for nitrous oxide on gold should be on the same order.

The equation used to determine C in our experiment (Eq. 3.7) already assumes wetting behavior. Additionally, it is possible that the data we used to determine C was not at sufficiently high pressures, as this would also affect the result.

In an attempt to correct for this apparent discrepancy, we repeated the derivation of D and T_w for the C value for water on gold. Although no longer exact, these calculations serve as an approximation to confirm our previous conclusions. This approximation did not change the prior conclusion that nitrous oxide wets gold at zero degrees Celsius.

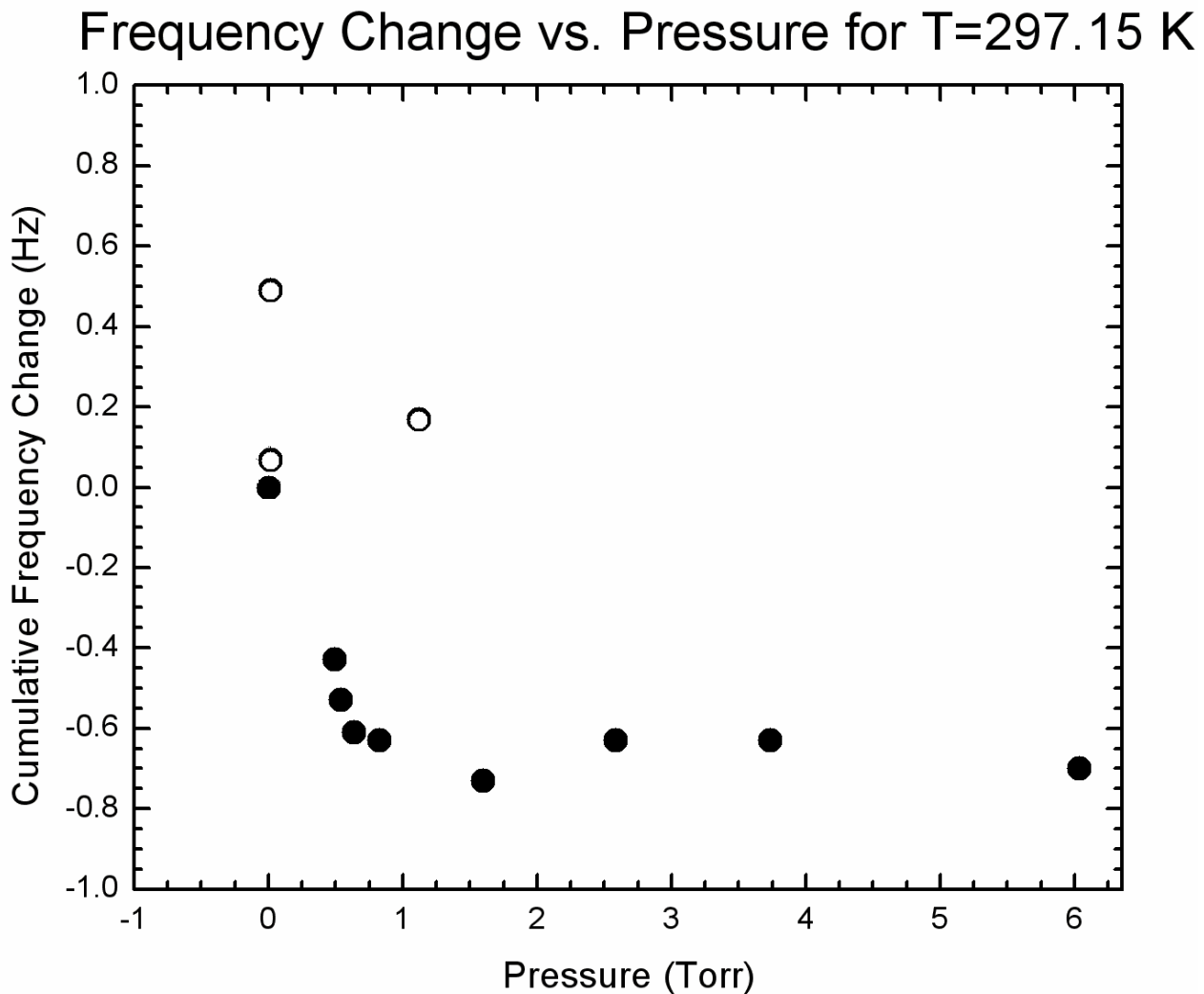
Additionally, it should be possible to arrive at a theoretical value for C for nitrous oxide on gold by comparing the relative polarizabilities of water and nitrous oxide:

$$\frac{C_{N_2O}}{C_{H_2O}} \propto \frac{\alpha_{N_2O}}{\alpha_{H_2O}} \tag{4.1}$$

Where α is the polarizability of the substances.

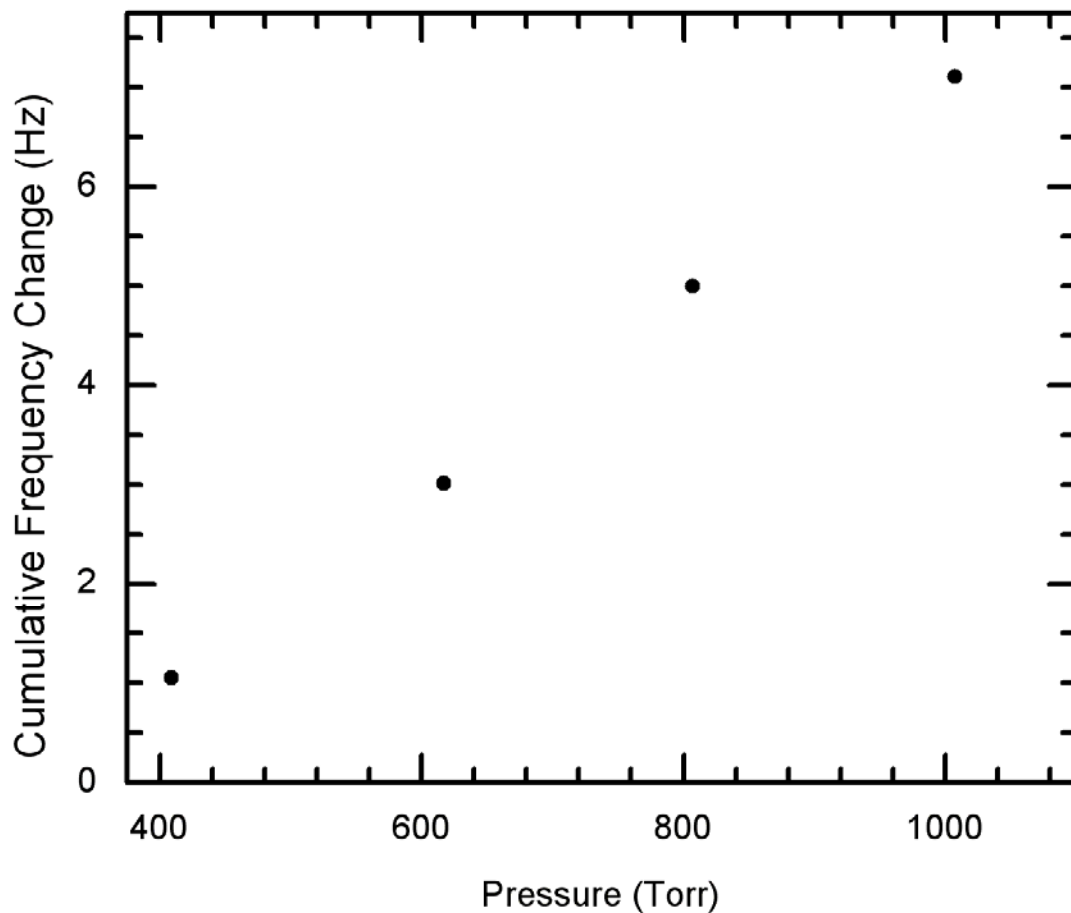
However, there are theoretical difficulties in calculating this directly.

The results of this experiment would be strengthened by repetition of the measurements for different temperatures, as was originally planned. Having minimized electrical noise and leaks in the apparatus, this should be easier than the initial set-up. Confirmations of this sort would require the introduction of a reliable method to control the temperature of the cell.



This is the data used in determining the value for df/dP at low pressures, which is used in finding D . Data that was not used is represented as a hollow circle; these data were erroneous as a result of electronic noise.

Change in Frequency vs. Pressure for T=297.15 K



This is the high-pressure data used to determine C. This regime is also represented in Fig. 3.2. The high-pressure limit is 1000 Torr (~1.3 atmospheres.)

APPENDIX B

```
function [] = EnergyIntegral( C, D, seed )

%this function integrates the potential energy
%function for given values of C and D
%make sure you use consistent units!
%Pass the function a value for seed that is close to the minimum
%of the potential function

%these are simply numeric values to simplify
%the later expression
alpha = -(4/27)*((C^3)./(D^2));

beta = C;

%this is the boltzmann constant times the temperature
%of the experiment, would need to be changed for different
%temperatures or units.
kT = 8.617E-5 * 273.15;

%this is the integrand
F = @(x) exp( (alpha./(x.^9) + beta./(x.^3))/kT )-1;
%this finds the zero, starting from the value for seed
x_min = fsolve(F,seed)

%these lines simply plot the equation so you can
%see what you're doing, subject to change depending on
%the equation
x=0.0001:.001:70;
plot(x,F(x))

%this performs the numeric integration, quadl should
%be a standard function for new versions of MATLAB
Q = quadl(F,x_min,x_min*100)
```

REFERENCES

- [1] E. Cheng, et al, *Helium Prewetting and Nonwetting on Weak-Binding Substrates*, **Physical Review Letters**, 67 (1007) (1991).
- [2] John W. Cahn, *Critical Point Wetting*, **Journal of Physical Chemistry**, 66(3667), (1977).
- [3] P. Taborek and J. E. Rutledge, *Novel Wetting Behavior of ^4He on Cesium*, **Physical Review Letters**, 68, 2184 (1992).
- [4] J. N. Israelachvili, *Intermolecular and Surface Forces*, 2nd ed. by (Academic Press, 1992).
- [5] NIST Chemistry Webbook for substance: Nitrous Oxide. webbook.nist.gov/chemistry/ accessed 4/24/07.
- [6] M. Gatica, X. Zhao, J. K. Johnson and M. W. Cole, *Wetting Transition of Water on Graphite and Other Surfaces*, **J. Phys. Chem. B** 108, 11704 (2004).
- [7] Stockbridge, C.D. *Resonance Frequency Versus Mass Added to Quartz Crystals*, in *Vacuum Microbalance Techniques*, Vol. 5, Ed. Klaus Behrndt, Plenum Press, NY (1966).
- [8] Stockbridge, C.D. *Effects of Gas Pressure on Quartz-Crystal Microbalances*, in *Vacuum Microbalance Techniques*, Vol. 5, Ed. Klaus Behrndt, Plenum Press, NY (1966).
- [9] Yang, L. *Quartz Microbalance Studies on Unsaturated Helium Films*, Ph.D. diss., University of California at Los Angeles, 1973.

- [10] Waegall, M. *Quartz Microbalance Apparatus for the Study of Wetting Phenomena*, MQP report, Worcester Polytechnic Institute, 2005.
- [11] R. Weiler, *Wetting Behavior of Nitrous Oxide Near its Critical Point*, MQP report, Worcester Polytechnic Institute, 2006.